Stochastic inversion of tracer test and electrical geophysical data to estimate hydraulic conductivities

James Irving[1,2] and Kamini Singha[3]

Received 1 July 2009; revised 17 June 2010; accepted 1 July 2010; published 9 November 2010.

[1] Quantifying the spatial configuration of hydraulic conductivity (K) in heterogeneous geological environments is essential for accurate predictions of contaminant transport, but is difficult because of the inherent limitations in resolution and coverage associated with traditional hydrological measurements. To address this issue, we consider crosshole and surface-based electrical resistivity geophysical measurements, collected in time during a saline tracer experiment. We use a Bayesian Markov-chain-Monte-Carlo (McMC) methodology to jointly invert the dynamic resistivity data, together with borehole tracer concentration data, to generate multiple posterior realizations of K that are consistent with all available information. We do this within a coupled inversion framework, whereby the geophysical and hydrological forward models are linked through an uncertain relationship between electrical resistivity and concentration. To minimize computational expense, a facies-based subsurface parameterization is developed. The Bayesian-McMC methodology allows us to explore the potential benefits of including the geophysical data into the inverse problem by examining their effect on our ability to identify fast flowpaths in the subsurface, and their impact on hydrological prediction uncertainty. Using a complex, geostatistically generated, two-dimensional numerical example representative of a fluvial environment, we demonstrate that flow model calibration is improved and prediction error is decreased when the electrical resistivity data are included. The worth of the geophysical data is found to be greatest for long spatial correlation lengths of subsurface heterogeneity with respect to wellbore separation, where flow and transport are largely controlled by highly connected flowpaths.

Citation: Irving, J., and K. Singha (2010), Stochastic inversion of tracer test and electrical geophysical data to estimate hydraulic conductivities, *Water Resour. Res.*, *46*, W11514, doi:10.1029/2009WR008340.

1. Introduction

[2] It is well recognized that the local spatial configuration of hydraulic conductivity (K) in heterogeneous geological environments is required for accurate predictions of contaminant transport [e.g., *Poeter and Gaylord*, 1990; *Scheibe and Yabusaki*, 1998; *Wen and Gómez-Hernández*, 1998; *Zheng and Gorelick*, 2003]. Traditionally, aquifer characterization has been based on the analysis of drill cores and/or the results of tracer and pumping experiments; however, these techniques are often inadequate for reliably characterizing heterogeneous aquifers because of an inherent gap that exists between them in terms of resolution and coverage [*Beckie*, 1996; *Hubbard and Rubin*, 2005]. Environmental geophysical methods have the potential to bridge this gap and improve characterization of subsurface variability. A trade-off associated with using such methods, however, is that they are sensitive to, and therefore give us information regarding, geophysical properties in the subsurface and not directly the hydrological properties of interest. As a result, a number of studies have attempted to link geophysical and hydrological variables through a variety of approaches, including the development of petrophysical relationships at the laboratory scale [e.g., *Archie*, 1942; *Topp et al.*, 1980; *Mavko et al.*, 1998], the numerical upscaling of such relationships to the field scale [e.g., *Moysey and Knight*, 2004; *Moysey et al.*, 2005; *Singha and Gorelick*, 2006; *Singha et al.*, 2007], and the use of statistical techniques such as cokriging of field-estimated collocated geophysical and hydrological properties [e.g., *Doyen*, 1988; *Cassiani et al.*, 1998]. Unfortunately, while relationships between a specific geophysical property and those of interest to hydrologists may exist on a scale-, site-, and/or facies-specific basis, they are often complicated, nonunique, and difficult to establish [*Day-Lewis et al.*, 2005; *Singha et al.*, 2007].

[3] To deal with the inherent difficulties associated with using geophysical methods to quantify hydrological properties as mentioned above, a number of approaches have been presented. One of these involves the use of multiple geophysical survey data, combined with either statistical regression analysis of collocated hydrological data and/or integrated petrophysical models, to reduce the estimation

[1]Faculty of Geosciences and Environment, University of Lausanne, Lausanne, Switzerland.
[2]Now at School of Engineering, University of Guelph, Guelph, Ontario, Canada.
[3]Department of Geosciences, Pennsylvania State University, University Park, Pennsylvania, USA.

0043-1397/10/2009WR008340

uncertainty associated with the use of a single geophysical method alone [e.g., *Ezzedine et al.*, 1999; *Chen et al.*, 2001; *Hubbard et al.*, 2001; *Garambois et al.*, 2002; *Linde et al.*, 2006a]. Another approach involves the use of one or more inverted geophysical data sets to divide or cluster the subsurface into a small number of zones having similar combinations of geophysical properties [e.g., *Beres and Haeni*, 1991; *Hyndman and Harris*, 1996; *Mukerji et al.*, 2001; *Moysey et al.*, 2003; *Tronicke et al.*, 2004]. Such zones are then assumed to represent different lithologies and possess distinct hydrological properties, which can be estimated either through the inversion of hydrological test data [e.g., *Hyndman et al.*, 1994, 2000; *McKenna and Poeter*, 1995; *Hyndman and Gorelick*, 1996; *Linde et al.*, 2006b], or through the analysis of collocated borehole hydrological measurements [e.g., *Paasche et al.*, 2006].

[4] Another promising means of using geophysical methods more effectively for hydrological characterization, and our focus in this paper, involves acquiring time-lapse geophysical data as changes occur in an aquifer as a result of some form of hydrological stress manifested as, for example, changes in soil saturation or the transport of solutes in the subsurface. Although geophysical data collected statically may provide little information regarding the distribution of a particular hydrological property, a set of dynamic data that are sensitive to changes in hydrological state variables, such as water content or salinity, can be much more uniquely tied to this distribution through the underlying hydrological process model [*Binley et al.*, 2002; *Kemna et al.*, 2002; *Binley and Beven*, 2003; *Day-Lewis et al.*, 2003; *Cassiani et al.*, 2004; *Lambot et al.*, 2004; *Cassiani and Binley*, 2005; *Singha and Gorelick*, 2005; *Koestel et al.*, 2008; *Chen et al.*, 2009]. One increasingly common way of utilizing such time-lapse geophysical measurements is through coupled or integrated inversion, where the numerical models for the geophysical and hydrological processes are linked together such that the geophysical data are inverted directly for the hydrological properties of interest. This research has been ongoing for petroleum applications [e.g., *Huang et al.*, 1997; *Kretz et al.*, 2004; *Wen et al.*, 2006] and has more recently become popular in hydrology [e.g., *Kowalsky et al.*, 2004, 2005; *Lambot et al.*, 2006; *Finsterle and Kowalsky*, 2008; *Jadoon et al.*, 2008; *Looms et al.*, 2008; *Lehikoinen et al.*, 2009; *Hinnell et al.*, 2010]. Coupled inversion has the significant advantage over separated or uncoupled inversion strategies in that it avoids the formation of geophysical images, which are subject to inversion artifacts and depend on the regularization of the geophysical inverse problem, both of which can significantly affect the hydrological estimates obtained [*Day-Lewis et al.*, 2005; *Ferré et al.*, 2009; *Hinnell et al.*, 2010]. However, while the coupled inverse problem has been an important step forward in quantifying hydrologic parameters, it has to a large extent been considered only within a deterministic or quasi-deterministic inversion framework, which does not allow for adequate exploration of the often strongly nonlinear and nonunique nature of the coupled system and corresponding model parameter and prediction uncertainties.

[5] In recent years, a number of papers have appeared in the geophysical literature that treat the complex data integration and inversion problem for spatially distributed subsurface properties in a fully stochastic manner using Bayes' Theorem [e.g., *Mosegaard and Tarantola*, 1995; *Bosch*, 1999; *Aines et al.*, 2002; *Eidsvik et al.*, 2002; *Ramirez et al.*, 2005]. Once thought computationally impractical, the results in these papers have demonstrated that with modern computational resources and state-of-the-art forward simulation and sampling algorithms, such stochastic data integration is feasible for real-world problems. In Bayesian inversion, the solution to the inverse problem is described as a joint posterior probability distribution for all model parameters, which is obtained by updating a prior distribution for these parameters using likelihood functions corresponding to the available sources of data. Samples from the posterior distribution (i.e., multiple feasible configurations of subsurface properties) can then be generated numerically using Markov Chain Monte Carlo (MCMC) sampling, as in general, explicit analytical expressions for this distribution are unavailable owing to the complexity of the associated forward models. When taken together, these posterior samples represent our uncertainty regarding the subsurface environment, and they can be used to make predictions within a stochastic context. Bayesian MCMC methods are naturally suited to dealing with the important issues of data worth and integration. They are also flexible in that they can incorporate any information that can be posed within a probabilistic framework. Although such methods have been applied in a wide variety of fields for many years, they have seen limited use in the field of hydrogeophysics.

[6] In this paper, we investigate the use of a Bayesian MCMC approach for the coupled inversion of saline tracer test concentration measurements and time-lapse electrical resistivity (ER) data for the purpose of estimating the spatial configuration and connectivity of K in the context of predicting solute transport. This is done between two boreholes in a saturated heterogeneous aquifer, and tested on two complex K fields having different facies correlation lengths. We focus here on testing the methodology numerically such that fundamental issues associated with the data integration and inversion can be examined in the case where the true subsurface model is known. Our research has conceptual similarities to other recent work on the fully stochastic inversion of dynamic hydrogeophysical data, in that we test randomly generated sets of model parameters with regard to how well they predict measurements, and then accept or reject them accordingly [*Binley and Beven*, 2003; *Cassiani et al.*, 2004; *Cassiani and Binley*, 2005; *Looms et al.*, 2008; *Hinnell et al.*, 2010]. However, an important difference is that we address here the problem of estimating a complex spatial distribution of subsurface properties, whereas most other work has focused on the determination of a small number of average parameters. In the studies cited above, for example, 1-D flow models were considered and continuous, uncorrelated prior parameter distributions could be assumed without overloading computational resources. In contrast, because we consider a substantially larger number of model parameters and perform forward simulations in multiple dimensions, simplification strategies are required to make the stochastic inverse problem computationally tractable. To this end, we explore a facies-based parameterization in our work. Another key difference between this and previous related efforts is that we account for uncertainty in the relationship between solute concentration and resistivity to address the fact that field-scale petrophysical relationships are dif-

ficult to establish. With few exceptions [*Kowalsky et al.*, 2005; *Finsterle and Kowalsky*, 2008], most previous work has considered such petrophysical relationships to be known and precise.

[7] The paper proceeds as follows. First, we outline briefly some general concepts of the Bayesian MCMC methodology used. Next, we describe our numerical experiment and the details of how we implement this methodology to integrate concentration and time-lapse resistivity data simulated from the two "true" K distributions. Finally, for each of the two cases, we examine the simplified binary K realizations generated from (1) the prior distribution, (2) the posterior distribution obtained by incorporating only the concentration measurements, (3) that obtained by incorporating only the resistivity measurements, and (4) that obtained using both the concentration and resistivity measurements. A key part of our testing is model validation. In this regard, the sets of realizations are evaluated against the corresponding true facies distributions to explore their ability to identify important transport pathways, and then in terms of their ability to predict a different solute injection/extraction experiment in the subsurface region.

2. Inversion Methodology

[8] Here we briefly outline the general concepts of the Bayesian MCMC methodology used in our work. For further details on its theory and application to geophysical inverse problems, see, for example, *Mosegaard and Tarantola* [1995], *Bosch* [1999], *Aines et al.* [2002], and *Ramirez et al.* [2005]. We begin by considering n sets of measured data $\{\mathbf{d}_1, \ldots, \mathbf{d}_n\}$ that each informs us in some way about the subsurface environment, and the vector $\mathbf{m}$ that contains the model parameters of interest, in our case the spatial configuration of K. Regarding $\mathbf{m}$ as a multivariate probability distribution, Bayes' Theorem can be used to update our initial state of knowledge about these parameters into a more refined state of knowledge given the available data. This powerful concept, which is the key behind Bayesian data integration and inversion, is expressed in terms of conditional probabilities as follows:

$$\underbrace{f(\mathbf{m} \mid \mathbf{d}_1, ..., \mathbf{d}_n)}_{\sigma} = k_1 \underbrace{f(\mathbf{d}_1, ..., \mathbf{d}_n \mid \mathbf{m})}_{L} \underbrace{f(\mathbf{m})}_{\rho}, \tag{1}$$

where ρ and σ are the joint prior and posterior distributions for the set of model parameters, respectively, k_1 is a normalization constant that ensures that the probability density function integrates to unity, and L is the joint likelihood function, which quantifies the probability of encountering the observed data sets given the model parameters. Assuming that observational uncertainties across the different data sets are statistically independent, an assumption which is commonly made in Bayesian joint inversion studies [*Mosegaard and Tarantola*, 1995; *Bosch*, 1999; *Aines et al.*, 2002; *Linde et al.*, 2007], then L in equation (1) can be expressed as a product of partial likelihoods corresponding to each data type, which yields the following formula for the posterior distribution:

$$f(\mathbf{m} \mid \mathbf{d}_1, ..., \mathbf{d}_n) = k_1 \left[\prod_{i=1}^{n} f(\mathbf{d}_i \mid \mathbf{m})\right] f(\mathbf{m}). \tag{2}$$

Each of the partial likelihoods, $f(\mathbf{d}_i|\mathbf{m})$, in turn involves a forward numerical simulation on the model parameters to produce a set of calculated data. That is,

$$L_i(\mathbf{m}) \equiv f(\mathbf{d}_i \mid \mathbf{m}) = \mathsf{M}(\mathbf{d}_i, g_i(\mathbf{m})), \tag{3}$$

where M denotes some general function of the misfit between the observed and calculated data ($\mathbf{d}_i$ and $g_i(\mathbf{m})$, respectively) and g_i represents the forward simulation process. For the case of independent, normally distributed data errors, which we assume in this study and discuss in more detail later, the partial likelihoods in equation (3) are given by:

$$L_i(\mathbf{m}) = k_2 \exp\left(-\frac{\left[g_i(\mathbf{m}) - \mathbf{d}_i\right]^{\mathrm{T}}\left[g_i(\mathbf{m}) - \mathbf{d}_i\right]}{\sigma_{d_i}^2}\right), \tag{4}$$

where k_2 is another normalization constant and $\sigma_{d_i}^2$ is the estimated variance of the measurement errors for data set $\mathbf{d}_i$.

[9] In general, because of the complexity of the forward calculations and high dimension of the model space in most realistic geophysical and hydrological data integration and inversion problems, there does not exist an explicit analytical expression for the posterior distribution described by equation (2). Instead, we have only a numerical process through which we can obtain the probability of occurrence of a particular set of model parameters. Nevertheless, this information can be exploited by numerical algorithms to efficiently generate samples from the posterior distribution, which can then be examined statistically to see how the various sources of data inform us about the subsurface environment. MCMC techniques are one particularly powerful and efficient class of such algorithms. In short, these methods involve stepping through a Markov Chain where, at each step, a test realization for $\mathbf{m}$ is proposed according the prior distribution, and is then either accepted or rejected using a random decision rule based on the realization's predicted data misfit and the misfit of the previously accepted model. After a certain "burn-in" period required for the procedure to stabilize and become independent of the initial starting realization, accepted samples drawn at regular intervals along the Markov Chain will represent independent realizations from the posterior distribution and will occur at a frequency corresponding to their posterior probability of occurrence. The random decision rule that we use for our MCMC work is based on a derivative of the *Metropolis et al.* [1953] algorithm derived by *Mosegaard and Tarantola* [1995], which is given by:

[10] 1. If $L_i^{new} \geq L_i^{old}$ (i.e., if the new model has equal or higher likelihood than the previously accepted one), then accept the proposed transition.

[11] 2. If $L_i^{new} < L_i^{old}$, then make a random decision to accept the proposed model with probability L_i^{new}/L_i^{old}.

[12] A more detailed discussion of the above decision rule and related MCMC convergence issues is provided in the work of *Mosegaard and Tarantola* [1995], *Aines et al.* [2002], and *Ramirez et al.* [2005]. A key consideration in our work is that, in the presence of multiple sources of data, the rule can be nested or staged such that each forward model is considered independently in the MCMC procedure in accordance with equation (2). That is, each proposed model need not be tested with regard to additional data sets if it has been tested and rejected on the basis of a data set

higher up within the nested structure. This results in significant computational savings. Another critical consideration in the practical application of Bayesian MCMC methods, especially when a large number of parameters is involved, is the decision of how to propose samples from the prior distribution as one moves along the chain [*Mosegaard and Tarantola*, 1995]. Clearly, if the change between the proposed and previously accepted models is too large from one iteration to the next, then the large difference in their likelihoods will virtually guarantee the proposal to be rejected. However, if the change is too small then the MCMC algorithm will be slow to converge and produce independent samples from the posterior distribution. In section 3, we discuss how all of these issues were dealt with in our example problem.

3. Application to Coupled Hydrogeophysical Inversion

[13] As mentioned, we explore numerically in this paper the application of a Bayesian MCMC approach to the problem of jointly inverting dynamic resistivity and concentration measurements, collected during a saline tracer test, to quantify transport pathways and improve hydrological predictions. To do this, we consider a two-facies system with variable K within facies, and we work with two example cases involving different facies and within-facies correlation lengths. Our examples are relatively simple to allow for effective testing of our proposed methodology, but they still contain a number of important complexities that make our results relevant to the eventual application of such a strategy to field data. Below, we describe our numerical experiment and the specific details of the MCMC procedure employed, with particular focus on the prior assumptions and steps taken to make it computationally tractable for the spatially distributed inverse problem. For the two example cases, we then examine the generated K realizations in terms of how well they estimate the true facies type at each location in the model, and more importantly in terms of their hydrological prediction ability.

3.1. Creation of "True" K Fields

[14] Two complex, heterogeneous K distributions at the local (~10 m) scale, having different facies correlation lengths, are considered as the "true" subsurface models to be estimated in this study. The fields are specified on a 10 m wide by 15 m deep simulation grid which is discretized using 0.5 m cells to yield a grid size of 20 × 30. To generate the K distributions, we used a combination of sequential indicator and sequential Gaussian simulation techniques. First, assuming a two-facies system, we used the SISIM program from GSLIB [*Deutsch and Journel*, 1992] to generate a facies distribution for each of the two cases. The facies were specified to have equal proportions and an exponential variogram model was employed for the simulations. For the first case (shown in Figure 1a), the horizontal and vertical correlation lengths of the facies were prescribed to be 3.5 m and 1 m, respectively. For the second case (shown in Figure 1c), they were prescribed to be 1.25 m and 0.5 m, respectively. Two facies systems such as these are reasonable for many fluvial or glaciofluvial sites, such as the intensively studied Cape Cod research site at the Massachusetts Military Base [*Hess et al.*, 1992] and the macrodispersion experiment site in Mississippi [*Adams and Gelhar*, 1992]. Note, however, that our proposed methodology is not at all limited to two-facies systems, and could easily be applied to greater numbers of facies with a corresponding increase in computational cost due to the greater number of parameters. Next, we simulated lognormal variability in K within each facies using the SGSIM program, also from the GSLIB toolbox. To do this, an exponential variogram model was again employed, and correlation lengths for ln(K) were set to be the same as those used for the sequential indicator simulation. For both models, facies 1 was prescribed a mean K value of 10 m/d, and facies 2 was prescribed a mean K value of 100 m/d. The variance of ln(K) within each facies was set to be 0.1. The resulting true K distributions are shown in Figures 1b and 1d. For the longer correlation length model in Figure 1b, facies 1 has minimum and maximum K values of 3.9 m/s and 20 m/d, respectively, whereas facies 2 has minimum and maximum K values of 44 m/d and 210 m/d. The total variance of ln(K) for this model is 1.4. For the shorter correlation length model in Figure 1d, facies 1 has minimum and maximum values of 4.2 m/d and 24 m/d, whereas facies 2 has minimum and maximum values of 33 m/d and 320 m/d. In this case, the total variance of ln(K) is also 1.4. Porosities in the simulation region were set to constant values of 0.2 and 0.3 for the low- and high-K facies, respectively, to approximate a sandy fluvial environment.

3.2. Tracer Test and ER Measurements

[15] The 20 × 30 models shown in Figures 1b and 1d were padded with 6 expanding cells along the bottom, left-, and right-hand sides to reduce the influence of the boundaries when conducting groundwater flow, solute transport, and resistivity simulations. Each cell increased in width and/or height by a factor of 1.3 going outward from the main grid, such that the outer boundary of the padded grid was a distance of 8 m away. For these synthetic examples, additional padding was not required to push away the boundary conditions as would be needed in a field setting. Steady state groundwater flow was simulated using MODFLOW-2000 [*Harbaugh et al.*, 2000] assuming no-flow boundaries at the top and bottom and fixed-head boundaries on the left and right sides such that a lateral head gradient of 0.02 was produced. A natural gradient tracer test through the model region was used for model calibration. One benefit of this type of test is that the size of the plume is large so its spatial variance is controlled by the subsurface heterogeneity rather than a forced flow field. For the tracer experiment, we consider two boreholes spaced 7.5 m apart in the subsurface region (Figure 1). A conservative saline tracer having a concentration of 1000 mg/L is introduced into the column of model cells representing the left borehole. This is meant to simulate the introduction of a fixed amount of tracer into the upgradient wellbore, which we consider to be fully screened. The background solute concentration in the rest of the model space was set to 10 mg/L. The initial volume of tracer is then left to travel through the subsurface and monitored for a period of 25 days. Conservative transport was simulated using the MT3DMS program [*Zheng and Wang*, 1999] with open boundaries on all sides. We assumed a longitudinal dispersivity of 0.8 m and a transverse dispersivity of 0.08 m,

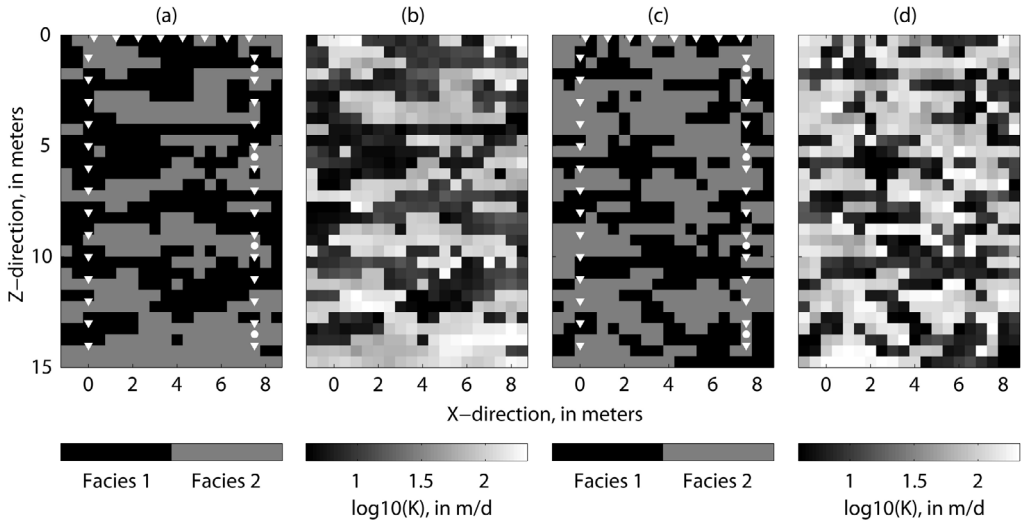

Figure 1. "True" facies and K distributions used to test the MCMC methodology, along with geophysical and hydrological instrument locations. (a) Facies distribution for longer correlation length case. (b) Corresponding $\log_{10}$(K) distribution. (c) Facies distribution for shorter correlation length case. (d) Corresponding $\log_{10}$(K) distribution. Thirty-six ER electrodes are shown as white triangles on the surface and in the boreholes, and four concentration sampling points are shown as white circles in the right-hand borehole.

which are reasonable for the scale of transport simulated here. Solute concentration data were recorded every 3 h at four measurement locations in the right-hand borehole (1.5, 5.5, 9.5, and 13.5 m depth) (Figure 1). Uncorrelated Gaussian random noise having a standard deviation of 5% of the mean value of the measurements was then added to these data.

[16] After modeling the tracer transport, the spatial distributions of solute concentration throughout the model region, in time increments of one day, were converted into distributions of electrical resistivity using two empirical relations. First, fluid resistivity in ohm-m, ρ_f, was obtained from the solute concentration in mg/L, C, using *Keller and Frischknecht* [1966]:

$$\rho_f \approx \frac{5000}{C}. \tag{5}$$

Next, ρ_f was related to the bulk resistivity, ρ_b, using Archie's Law [*Archie*, 1942]:

$$\rho_b = \rho_f \phi^{-m}, \tag{6}$$

where ϕ is the total porosity (equal to 0.2 or 0.3 for facies 1 or 2, respectively) and m is the Archie cementation exponent which we set equal to 1.3 to represent an unconsolidated sand [*Mavko et al.*, 1998; *Schön*, 1998; *Knight and Endres*, 2005]. Archie's Law is the most commonly used relationship to describe the connection between bulk and fluid resistivity. Having the distribution of electrical resistivity throughout the model region in time, we then simulated the collection of time-lapse electrical resistance measurements, once per day, using FW2_5D, a MATLAB-based 2.5-D resistivity modeling code [*Pidlisecky and Knight*, 2008]. Each borehole was assumed to be instrumented with 14 resistivity electrodes separated by 1 m spacing, with 8 surface electrodes spaced between the boreholes (Figure 1). Four hundred and eighty-five quadripoles, with 18 unique current pairs to minimize the number of forward models required, were simulated using crosswell and in-well current dipoles. From the resistance measurements, V/I, we calculated the apparent resistivity, ρ_a, as follows:

$$\rho_a = G\frac{V}{I}, \tag{7}$$

where V is the simulated voltage, I is the current used to drive the measurement, and G is a geometric factor used to correct for the geometry of the electrodes [*Keller and Frischknecht*, 1966]. While we could have worked directly with resistance data for this study, using apparent resistivities made the addition of noise more straightforward. In that regard, uncorrelated Gaussian random noise having a standard deviation equal to 5% of the mean value of the measurements was added to the apparent resistivity data. Although the noise added to both our concentration and resistivity data sets is uncorrelated, which is a standard assumption in synthetic studies in both geophysics and hydrology, it is important to note that our MCMC procedure involves the much more complicated case of strongly correlated errors as a result of approximations made in the inverse problem. These approximations, described in section 3.3, result in structural model error for our system, which acts together with data uncertainties to provide a challenging test case.

3.3. Prior Distribution and Assumptions

[17] The forward modeled tracer concentration and time-lapse resistivity data described above were inverted within a Bayesian MCMC framework to generate multiple feasible spatial configurations of K in the unpadded model region. The use of MCMC methods for complex geophysical and hydrological data integration for spatially distributed properties is a combinatorially massive problem. As mentioned,

previous stochastic inverse approaches have generally involved a small number of estimated parameters and fast 1-D models, which meant that continuous prior distributions for these parameters could be used without overloading computational resources. In our work, this is not the case, and a key element of our approach is thus to limit, as much as possible, the number of subsurface configurations that must be tested through the data likelihood functions, whose evaluation involves computationally expensive forward model calculations. We do this by efficiently parameterizing the model space into facies and by incorporating as much knowledge as possible about the 2-D system into a fast sampling algorithm for the prior distribution. Lithology forms the "base representation" for our inversion methodology [*Aines et al.*, 2002]. The reasons for this are (1) geophysical and hydrological properties of subsurface materials are a direct result of lithological characteristics; (2) petrophysical relationships, which are often rather uninformative when considered independent of lithology, can become substantially more useful when grouped according to soil or rock type [*Prasad*, 2003]; and (3) prior geological knowledge is generally expressed in terms of relationships between lithologic or facies units, rather than between geophysical or hydrological properties. To decide on the number and type of lithologies to use in the MCMC data integration in the field, one could rely on prior knowledge of the geological environment, borehole logging or core data, or possibly the results of cluster analysis performed on a suite of already-inverted or processed geophysical images. Indeed, recent work in the latter category has suggested that, although individual geophysical images may not be clearly linked to hydrological properties and are prone to inversion artifacts and the effects of regularization, there is much potential to use together the images obtained from multiple techniques to cluster the subsurface into likely groups of lithologies [*Moysey et al.*, 2003; *Tronicke et al.*, 2004; *Paasche et al.*, 2006].

[18] For the prior distribution in our numerical example, we assume to have a basic understanding of lithology in the simulation region. Specifically, we assume to know that we are dealing with a two-facies system where we have information regarding the mean K and porosity values of each facies, but no knowledge of the variance of K. Information regarding mean K and porosity could be discerned, for example, from borehole flowmeter and neutron log data, respectively. We then use sequential indicator simulation to efficiently generate binary configurations of K that are tested in the MCMC procedure with regard to how well they allow us to predict the measured data. While simulation methods based on two-point statistics may produce inadequate measures of connectivity [*Knudby and Carrera*, 2005], sequential indicator simulation has been used with success to model spatial continuity for class-specific patterns [e.g., *Goovaerts*, 1997]. Realizations are simulated using the SISIM program from GSLIB, keeping the gridblock size in the area of interest at 0.5 m. Uncertainty in the horizontal facies correlation length, a_x, is accounted for by allowing it to vary between iterations according to a uniform distribution. For both our longer and shorter correlation length examples (with true a_x equal to 3.5 m and 1.25 m, respectively), the lower and upper bounds of this distribution were set to 0.5 m and 10 m. This represents a broad range which, considering that the distance between the boreholes is only 7.5 m, means that we assume basically no knowledge of the horizontal correlation structure. We assume that the vertical correlation length of the facies, a_z, can be estimated from borehole data [*Hess et al.*, 1992], although this could certainly be placed as another unknown in the inversion procedure. The subsurface dispersivity is considered known, on the basis of what would have been estimated in the "true" field tracer experiment.

[19] Because of the inherent difficulties in relating geophysical and hydrological variables, especially at the field scale, we also account for uncertainty in the relationship between solute concentration and resistivity in our work. This is accomplished by assuming that Archie's Law in equation (6) holds, but that the value of the cementation exponent, m, is unknown and allowed to vary between MCMC iterations. As mentioned, Archie's Law is the standard relationship used to link the bulk and fluid resistivities in porous materials. By assigning m a uniform distribution with lower and upper bounds of 1.1 and 1.5 (true value 1.3), we capture a realistic range of values expected in unconsolidated materials and allow for significant uncertainty. In section 3.4, we explain in more detail how the uncertainty in m was dealt with in the MCMC procedure.

[20] It is important to note that, because we assume a binary K field in our generation of test realizations from the prior distribution (with K for each facies simply equal to the mean value), our inversion considers a case that is considerably simpler than in reality where K varies within each facies (Figures 1b and 1d). This is a critical part of our MCMC procedure, as it drastically reduces the number of potential configurations for K, thus making the solution of the inverse problem computationally tractable. For the application of MCMC methods to problems with many parameters, the number of degrees of freedom must be limited as much as possible [*Ramirez et al.*, 2005]. Our assumption is consistent with the limited amount of information that one might be able to estimate in a field setting. However, making the assumption introduces model structural error into our inversion, in the sense that our true K model could never be tested given the simplified parameterization. Nonetheless, we shall see that this parameterization still allows posterior realizations of K to be generated that allow for an improvement in hydrological predictions. Indeed, a key goal of this study was to investigate whether assuming a simple spatially distributed K system, where constant K values within each facies are enforced to make the problem computationally feasible, would allow us to still identify flow pathways and reduce hydrological prediction uncertainty using the geophysical data when the real K configuration was considerably more complex. In section 5, we briefly discuss the difficult issue of model error resulting from this assumption and its impact on uncertainty assessment.

3.4. MCMC Procedure

[21] Figure 2 is a flowchart illustrating the various stages involved in our MCMC inversion of the tracer concentration and time-lapse resistivity measurements. The first step in this procedure, after drawing a random value for the lateral facies correlation length, is to generate a binary test configuration for K consistent with the prior distribution. As mentioned, we do this using the SISIM program from GSLIB. If this is the first iteration of the MCMC procedure,

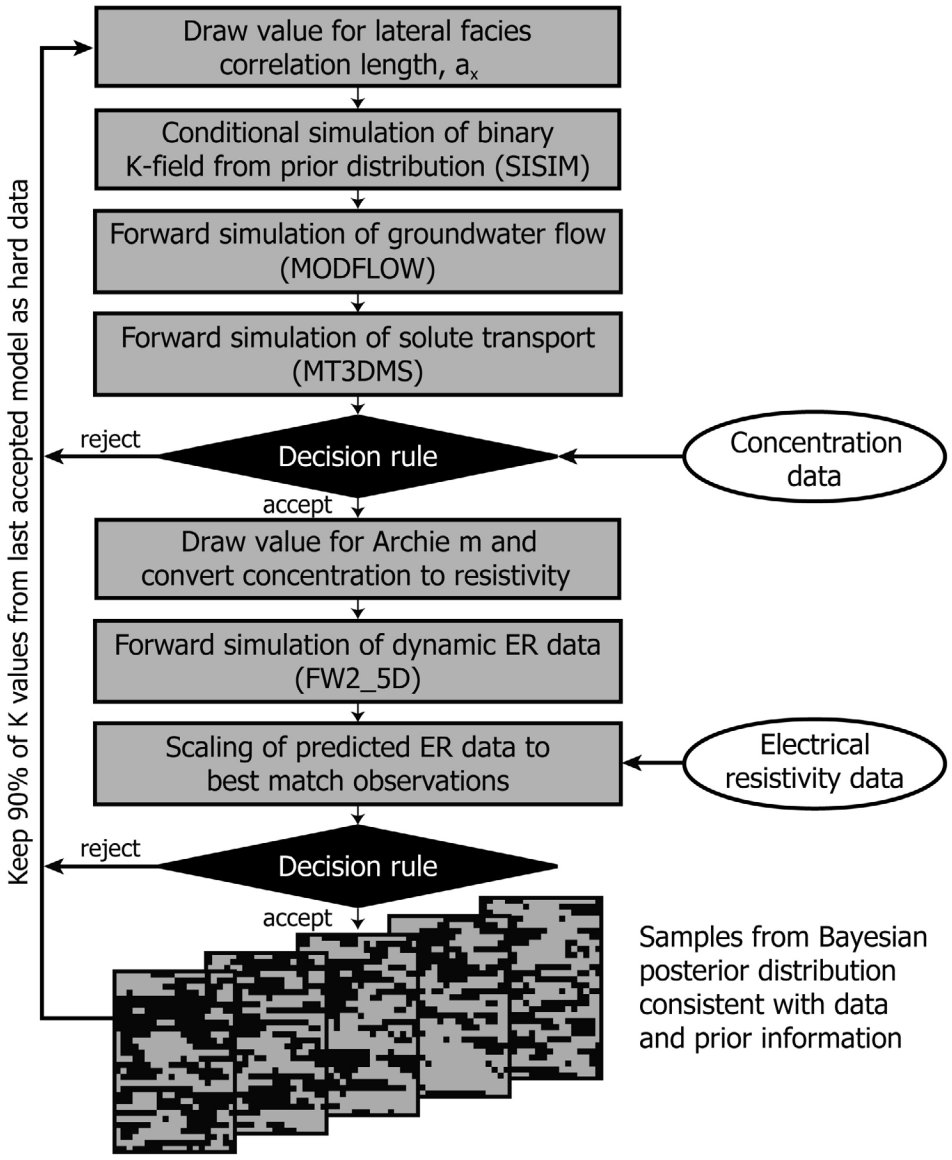

Figure 2. Flowchart outlining the MCMC procedure that we use to jointly invert the dynamic tracer concentration and apparent resistivity data for multiple binary realizations of K, effectively sampled from the Bayesian posterior distribution.

then no conditioning to previously simulated points is required and the configuration is accepted outright as the first model in the Markov Chain. Otherwise, it is important to ensure that the proposed model is not too different from the previously accepted model such that the ratio of their likelihoods allows a realistic chance of the proposal to be accepted [*Mosegaard and Tarantola*, 1995]. In our case, we ensure minimal model perturbations from one iteration to the next by changing only a randomly selected 10% of the model cells. The other 90% are set as hard data in the SISIM program. Doing this has the desired effect of significantly increasing the rate of acceptance of the proposed models; however, it clearly means that the accepted models, when taken sequentially down the posterior Markov Chain, will be similar and thus not statistically independent. Nevertheless, accepted realizations taken every so many iterations down the Markov Chain can be treated as independent samples from the posterior distribution. Our decision to keep 90% of model cells as hard data between iterations was based on ensuring a suitable rate of model acceptances in the MCMC procedure. This value clearly affects the lag at which we extract independent samples from the posterior chain, in that an increase in the former requires an increase in the latter. A lag value of 100 was determined to be sufficient for independent posterior sampling through analysis of when the average correlation coefficient between realizations in the Markov Chain decreased to a limiting background value.

[22] Once a test K configuration has been generated, we then calculate its predicted data. First, groundwater flow is simulated using MODFLOW to yield the steady state distribution of hydraulic head in the subsurface region. This is

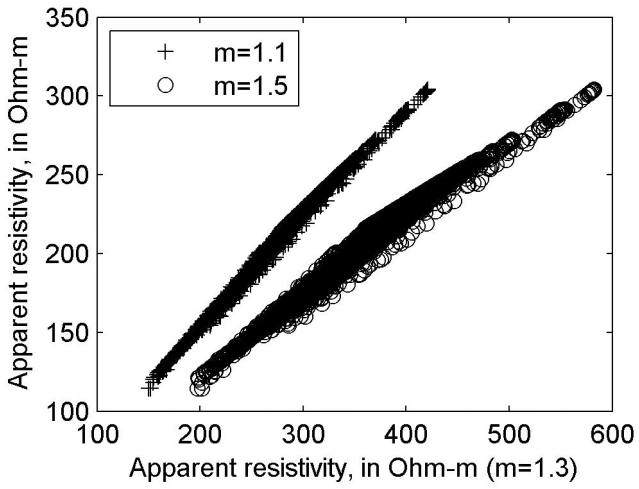

Figure 3. Scatterplot showing predicted versus true apparent resistivity data values corresponding to the subsurface K field from Figure 1b, but using two incorrect values for the Archie *m* exponent to compute the predicted data.

then used by MT3DMS to simulate the natural-gradient tracer experiment, which results in a set of predicted solute concentration curves at the four measurement ports in the right-hand well, as well as the predicted spatial distribution of concentration in time. In the first MCMC accept/reject step, the likelihood of the test model is computed from the misfit between the measured and predicted concentration data according to equation (4). Only if the model is accepted using our Metropolis-based decision rule do we continue down the flowchart and consider how well it predicts the measured resistivity data. If the model is rejected, then we return to propose a new configuration of K consistent with the prior distribution and conditioned to a random 90% of cells from the previously accepted model. Note how in this way the decision rule is staged such that the different types of observed data are considered separately; thus additional forward models need not be computed if the model is rejected on the basis of a particular data set.

[23] To calculate the predicted time-lapse apparent resistivity data for the test K configuration using the FW2_5D code, we must first convert the predicted distributions of solute concentration into electrical resistivity. This is done using equations (5) and (6) and a randomly drawn value for the Archie *m* exponent to allow for uncertainty in our knowledge of the true petrophysical relationship at the scale of a grid cell. Once again, the misfit between the predicted and true apparent resistivity data is used to compute the model likelihood and decide whether or not to accept the proposed realization. However, an important step that we perform before evaluating the apparent resistivity data misfit, which we have found allows us to deal effectively with the uncertainty in *m* in the inversion, is to scale the predicted data such that its least squares misfit with the measured data is minimized. That is, before deciding to accept or reject the proposed model, we scale the predicted resistivity data by a constant factor that provides the best match with the observed measurements. We base this step on the following logic: Without scaling the data, an incorrect value of *m* will result in predicted apparent resistivity measurements that differ in overall magnitude from the true data, even for the correct configuration of subsurface K, because of an incorrectly specified concentration/resistivity relationship. This means that the test model will most likely be rejected, even if it represents the correct K field, which in turn means that the MCMC procedure will be slow to produce accepted samples from the posterior distribution. However, we have found that apparent resistivity data computed using the incorrect value of *m* still contain useful information regarding the true K field, and often differ from the data produced using the correct value of *m* by an approximately constant factor. This is illustrated in Figure 3, where we plot the predicted versus true resistivity data corresponding to the true K field from Figure 1b, but using incorrect *m* values of 1.1 and 1.5. These values represent the lower and upper bounds of our uniform prior distribution for this parameter. Despite an incorrect *m* value, the predicted data are approximately linearly related to the true data, which suggests that scaling them would produce a set of measurements which could still provide useful information regarding the configuration of K. We find that including the data scaling step into our MCMC procedure results in an efficient means of dealing with an uncertain concentration/resistivity relationship. However, this scaling assumes that fluid resistivities are well constrained. Other methods for correcting for an uncertain *m* are possible.

[24] After scaling the predicted resistivity data and calculating the model likelihood, we use again the Metropolis-based decision rule to determine whether or not to accept the proposed K configuration. If the configuration is accepted, then it is added to the chain of realizations which, after a prescribed burn-in period, represent samples from the Bayesian posterior distribution consistent with both data sets. These can then be analyzed in terms of their ability to identify highly connected flowpaths and make transport predictions, which we discuss next. Otherwise, we return to propose another test configuration consistent with the prior distribution and conditioned to be a small perturbation from the previously accepted model. In our implementation of the above MCMC algorithm, we let the procedure run until 150,000 realizations of K had been accepted, which we found was sufficient to allow for meaningful posterior analysis. On a 2.4 GHz computer with 8 GB RAM, each flow simulation took ~0.1 s, each transport simulation ~1 s, and each electrical flow simulation ~2.5 s, which meant that running a single inversion procedure required about one week of CPU time. To determine at what point the MCMC algorithm converged to properly represent the posterior distribution (i.e., the burn-in period), beyond which the effects of the initial starting realization have been "forgotten" and stationarity has been achieved, we ran 4 simultaneous Markov Chains using completely different random starting models. Burn-in was estimated on the basis of the point where the variance between chains was similar to the variance seen within each chain [e.g., *Gelman and Rubin*, 1992; *Aines et al.*, 2002]. Examination of the mean and variance of each model cell for the different chains after this period also confirmed convergence. As mentioned previously, before analyzing the posterior realizations (presented in section 3.5), every 100th realization was extracted from the chain of accepted models to produce a set of independent posterior samples. The first 300 of these samples were discarded as part of the burn-in period, leaving 1200 samples for analysis.

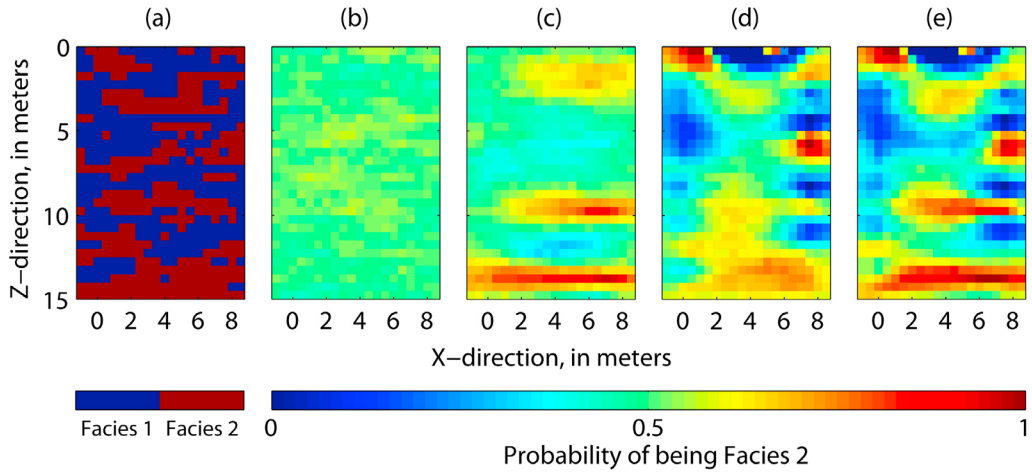

Figure 4. Results of MCMC inversion procedure for the longer correlation length K field shown in Figure 1b. (a) True facies distribution. (b) Probability of being in facies 2 computed from realizations generated from the prior distribution. (c) Probability of being in facies 2 computed from posterior realizations generated considering only the concentration measurements, (d) only the ER measurements, and (e) the concentration and ER measurements together.

3.5. Results

3.5.1. Generated Realizations

[25] We first show the results of our MCMC inversions in terms of how well the generated posterior realizations are able to capture the transport pathways present in the true facies distributions shown in Figures 1a and 1c. Figures 4a and 5a show again these distributions for the longer and shorter correlation length examples, respectively. In Figures 4b–4e and 5b–5e, we show maps of the probability of being in facies 2, which was calculated on a cell-by-cell basis from the posterior MCMC realizations that were generated by incorporating different amounts of information into the inversion procedure. Regions that are blue represent a high probability of being in facies 1, whereas regions that are red represent a high probability of being in facies 2. Green regions indicate places where, given the data used in the inversion procedure, we cannot clearly distinguish which facies is present.

[26] In Figures 4b and 5b, we show the probabilities computed when only the prior information was used to generate the K realizations. In other words, no data were used to condition the realizations in this case, and every binary random field created using SISIM was accepted. For both the short and long correlation length examples, the probabilities of being in facies 1 and facies 2 are approximately equal everywhere. This is expected because our prior distribution does not contain any information regarding what facies is present at each point in space; it only specifies that the two facies will be correlated according to an exponential variogram model having a vertical correlation length of 0.5 or 1 m, depending on the field considered, and an uncertain horizontal correlation length between 0.5 and 10 m. Here, we can verify that the prior simulation procedure is not biased regarding the spatial location of facies 1 and 2.

[27] Figures 4c and 5c show the probabilities obtained from the posterior accepted realizations when only the tracer concentration measurements were considered as data in the MCMC inversion procedure. As a result, the realizations in this case are conditioned by both the prior distribution and concentration data, but not by the time-lapse ER data. In Figure 4c, we see that, by adding the concentration data (collected at 1.5, 5.5, 9.5, and 13.5 m depth), we are able to correctly identify three high-K pathways near the top, middle, and bottom of the true model. These pathways are indicated by regions of higher probability of being in facies 2, meaning a predominance of this facies at the three locations in the output realizations. Because of the location of the measurements, the pathways occur around 1.5, 9.5, and 13.5 m depth, although in the true model the uppermost high-K pathway lies slightly deeper, around 2 m depth. For the case of the shorter correlation length K model (Figure 5c), however, we observe quite different behavior. In this case, in the majority of the image, with the exception of a small region in the lower right-hand corner where facies 1 is correctly identified in the majority of realizations, the calculated probabilities are uninformative and very much like those computed from the prior realizations. The main reason for this is the lack of horizontally well-connected and continuous high-K regions in Figure 5a, as opposed to Figure 4a. Consequently, the tracer breakthrough times for the four concentration measurements are quite similar, and do not suggest the need for consistently high- or low-K regions across the model. In addition, because of the shorter correlation length, it is possible to have high-K pathways that are present in the output realizations, but are not consistently at the same location such that they are seen in the probability plots in Figures 4 and 5. This is a weakness of representing our results in terms of cell-by-cell calculated probabilities. Finally, note that the lack of horizontal variability seen in Figures 4c and 5c shows the limitations of the sparse concentration measurements in terms of the information that they provide regarding the spatial structure of K.

[28] In Figures 4d and 5d, we show the probabilities calculated from the output realizations when only the dynamic apparent resistivity measurements were considered in the stochastic inversion procedure. Again, resistivity was linked to solute concentration in the coupled hydrogeophysical model using Archie's Law with an uncertain m

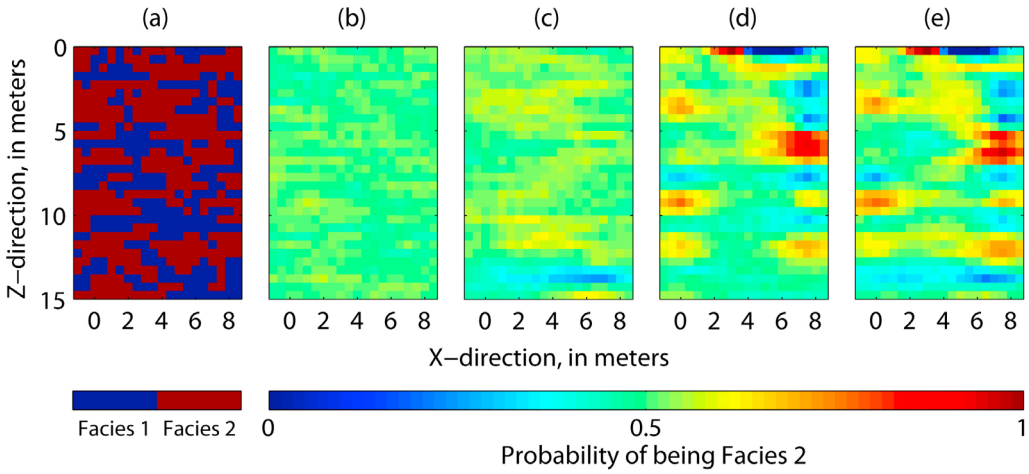

Figure 5. Results of MCMC inversion procedure for the shorter correlation length K field shown in Figure 1d. (a) True facies distribution. (b) Probability of being in facies 2 computed from realizations generated from the prior distribution. (c) Probability of being in facies 2 computed from posterior realizations generated considering only the concentration measurements, (d) only the ER measurements, and (e) the concentration and ER measurements together.

exponent. In contrast to the case where only the concentration measurements were used, notice here the generally excellent reproduction of the correct facies distribution around the top and sides of the model, which correspond to the location of the ER electrodes where the sensitivity of the resistivity method is highest. This is especially the case for the longer correlation length model in Figure 4d. Near the center of the model, the ER measurements also provide us with some important information regarding the distribution of facies, especially the high-K pathways, which are more easily resolved as they provide a preferential pathway for current when the solute travels through them and they become electrically conductive. In Figure 4d, the high-K regions near the bottom of the model are quite consistently represented in the output realizations. In Figure 5d, albeit less evident, the high-K region in the upper right part of the model is reasonably well captured.

[29] Finally, Figures 4e and 5e show the probabilities obtained when both the concentration and ER data sets were inverted together using the staged MCMC framework described in section 3.4. In general, these probability plots visually resemble a combination of the information in Figures 4c, 4d, 5c, and 5d, which is to be expected. Comparing Figure 4e with the true facies model in Figure 4a, we see that by incorporating both types of data into the inversion procedure, we are much better able to consistently delineate the spatial connectivity in facies in comparison with using either data type alone for the larger correlation length case. Conversely, in Figure 5e, the results are much less clear. Here we see a much greater amount of ambiguity regarding the facies distribution, except near the electrode locations where the resistivity data provide much information. Nevertheless, considering the relatively complex nature of the heterogeneity in Figure 5a, many of the low- and high-K regions in the true model are captured in a large number of realizations, which is manifested as the light-blue and yellow regions seen in Figure 5e, respectively. Again, these pixel-by-pixel probability plots are not able to show captured K pathways that change position between realizations; therefore, such plots are not the best representation of how well the generated realizations capture K connectivity. The true validity of the posterior MCMC realizations can only be assessed through evaluating their predictive ability in the context of a different transport experiment, the results of which we show in section 3.5.2.

[30] In Table 1, we quantify the results in Figures 4 and 5 through the cumulative squared difference between the probabilities shown and the indicator variable for being in facies 2 corresponding to the true facies distribution. At locations in Figures 4a and 5a where facies 2 is present, the indicator variable equals one. Otherwise it takes on a value of zero. The cumulative squared difference between the probabilities and this variable (summed over all cells in the model domain) is thus a measure of how well our realizations match the true binary facies configuration in each case. Note that all of the results in Figures 4 and 5 are well summarized in Table 1, which shows a gradual reduction in the cumulative squared difference measure as more information is incorporated into the MCMC inversion procedure. As was observed in Figures 4 and 5, this reduction is greatest for the longer correlation length case. In the shorter correlation length case, the measure indicates that the resistivity plus concentration data do not do a significantly better job of identifying facies than the resistivity data alone.

3.5.2. Model Validation

[31] We now validate the performance of the various sets of binary K realizations discussed above with regard to their ability to predict the results of a different transport experiment through the subsurface region. It is important that the test employed during model validation is notably different from the one used to calibrate the model parameters, as the sets of realizations obtained through the MCMC procedure are conditioned to those particular calibration data. As a result, in contrast to the natural gradient experiment used to estimate K, we now test the generated realizations in the context of a doublet test, where we inject tracer having a concentration of 1000 mg/L into a well located 0.5 m behind the source well used for the natural gradient test at a rate of 1 gpm, and we extract it from the right-hand well at the same rate. The natural hydraulic head gradient of 0.02 is

Table 1. Cumulative Squared Difference Between the Probabilities Plotted in Figures 4b–4e and 5b–5e and the Indicator Variable in Facies 2 Corresponding to Figures 4a and 5a[a]

Example	Prior Distribution	Concentration Data	Resistivity Data	Concentration Plus Resistivity Data
Long correlation	151.3	144.5	121.9	**117.1**
Short correlation	150.7	148.1	137.4	**135.7**

[a]Boldface values represent the smallest values.

significantly perturbed by the injection/extraction during the 25 day period. As in the natural gradient test, the solute concentration is measured every 3 h in the right-hand well at 1.5, 5.5, 9.5, and 13.5 m depth.

[32] Figures 6 and 7 show the solute concentration curves obtained at the four sampling ports for each of the sets of realizations considered earlier, for the long and short correlation length K models, respectively. The gray curves show the predictions for the whole set of realizations, whereas the thin black solid and dashed lines show the mean prediction plus and minus two standard deviations. The thicker black lines show the concentration curves obtained by modeling through the true K realization (i.e., the concentration behavior that we would like to predict). Note that it takes ~10 days for the concentration to peak at the downgradient well. The concentration does not reach a peak value of 1000 mg/L because there are multiple pathways along which the tracer can travel and these pathways do not become saturated with solute before it leaves the system. In Table 2, we summarize the results in Figures 6 and 7 and quantify the predictive ability of our realizations with two measures. The first is the root mean square (RMS) difference between the mean predicted and true concentration curves, which clearly quantifies the accuracy of the average predicted behavior. The second is the average standard deviation of the predictions, taken over all time steps, which is a summary measure of the prediction uncertainty. The lowest values in each case are highlighted.

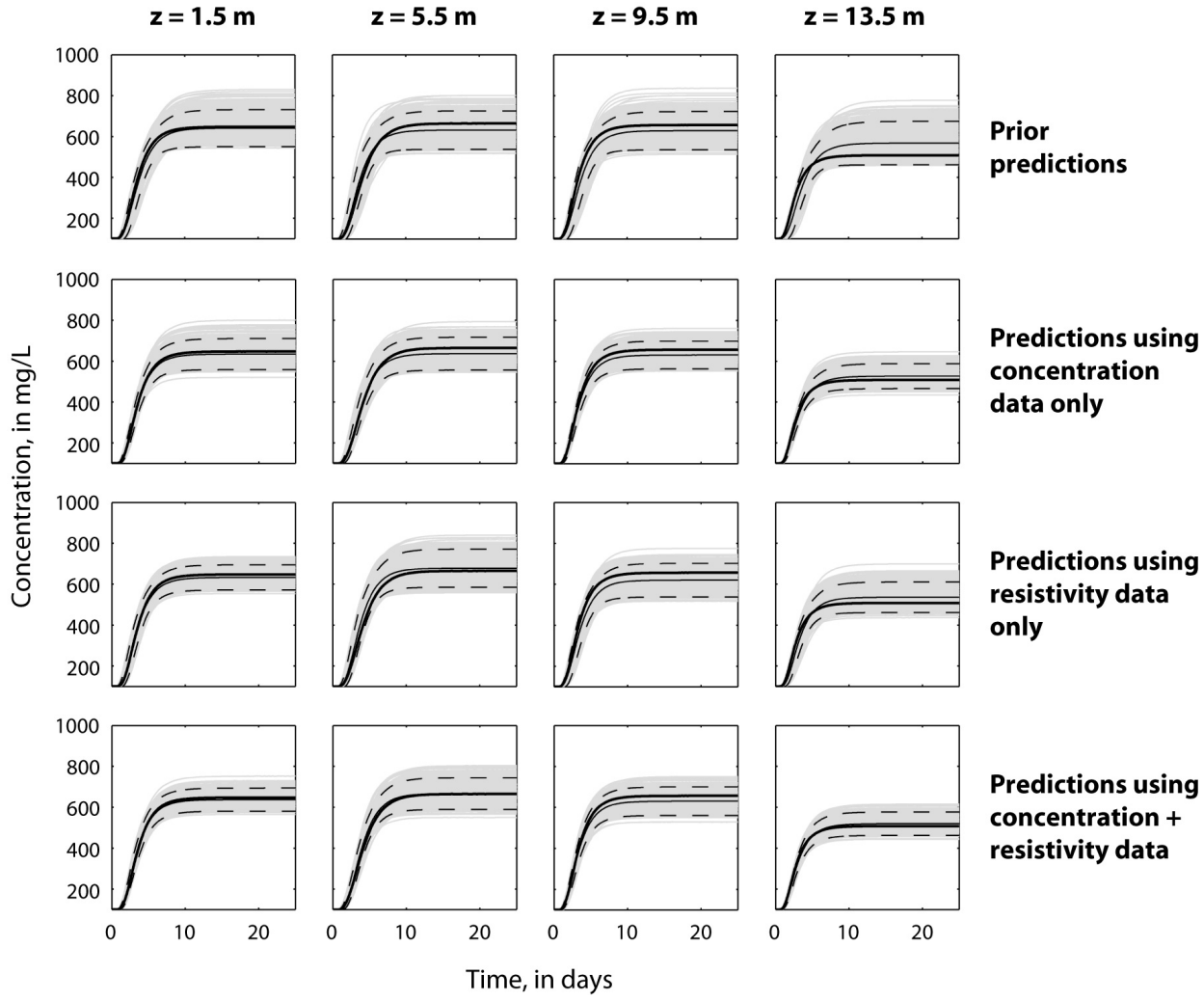

Figure 6. Predicted tracer concentration curves for the new injection test, obtained using the different sets of realizations from Figure 4. The thick solid lines show the curves obtained by modeling through the "true" K-field in Figure 1b, whereas the thin solid lines show the corresponding mean predicted behavior. The dashed lines show plus and minus two standard deviations around the mean predicted curve.

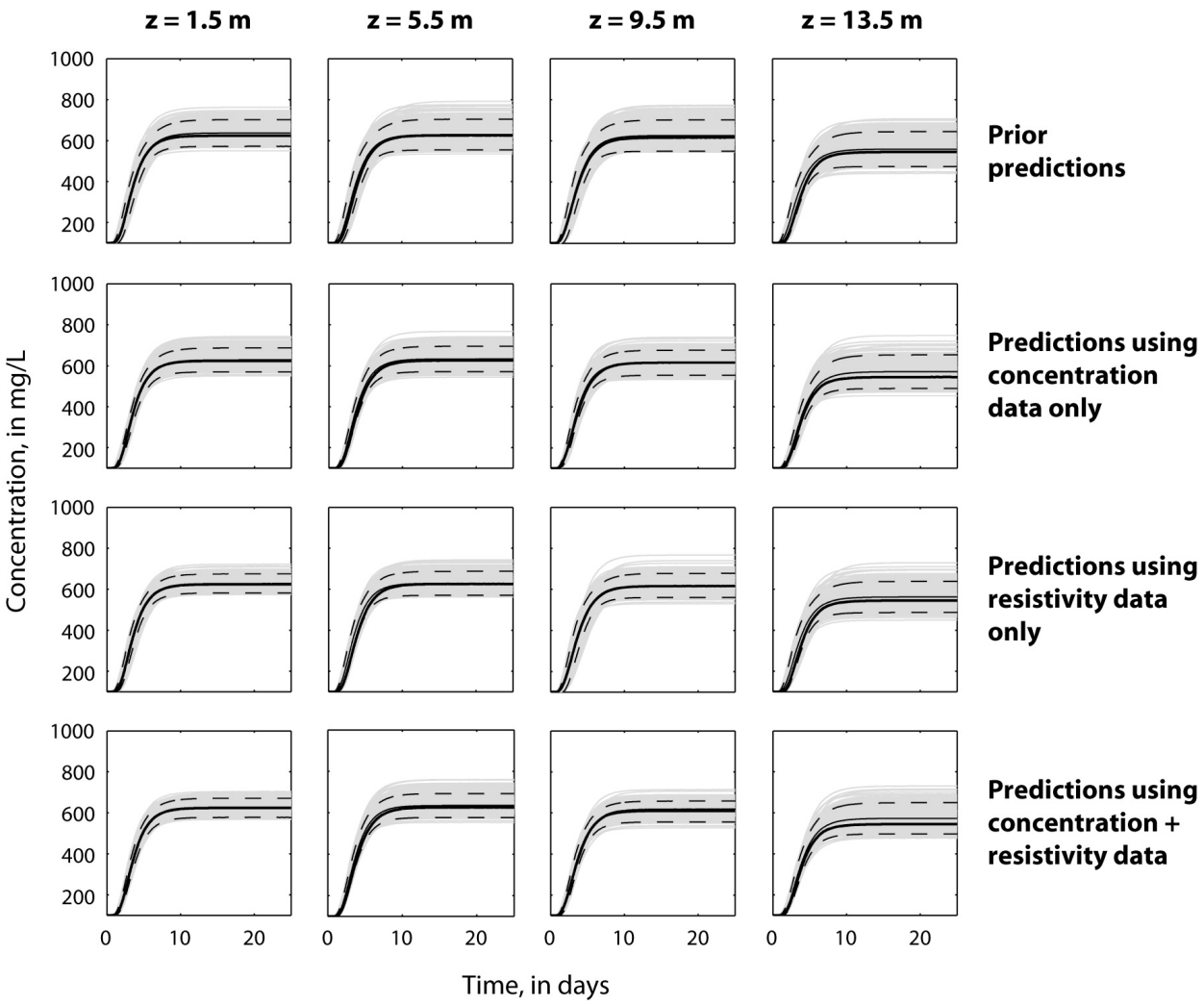

Figure 7. Predicted tracer concentration curves for the new injection test, obtained using the different sets of realizations from Figure 5. The thick solid lines show the curves obtained by modeling through the "true" K field in Figure 1d, whereas the thin solid lines show the corresponding mean predicted behavior. The dashed lines show plus and minus two standard deviations around the mean predicted curve.

[33] The sets of realizations generated from the prior distribution for the longer correlation length K model (i.e., not incorporating any of the measured data into the MCMC procedure) result in sets of predicted concentration curves with a relatively large spread about the true curve for all four sample ports (Figure 6). Given the results in Figure 4, this is expected because the prior contains no information regarding the spatial location of facies. The two standard deviation limits in this case are quite broad, and the mean predictions do not in general match the true curves in terms of solute arrival time or maximum predicted concentration. As a result, we can conclude that our prior information alone does not allow for reasonable predictions of hydrological behavior in the synthetic aquifer. In examining the predictions obtained by incorporating only the tracer test concentration data into the inversion procedure, the spread of the predictions becomes noticeably reduced, and the mean predicted behavior matches more closely the true curves for all sample ports (Table 2). Similarly, the predictions obtained from the realizations generated by considering only the time-lapse ER data also generally show a reduction in the spread of the predictions about the mean curve compared to the prior, and a closer match in many cases of the mean behavior to the true concentration curves. Both data sets clearly offer important information toward the prediction of solute transport through the model region. When both the concentration and ER data are considered together in the MCMC inversion procedure, we have the best results; for all of the sample ports, there is a significant reduction of uncertainty in the predicted behavior compared to the prior, and the mean predicted concentration curves match much better the true ones. Indeed, the minimum average prediction variance and best match to the true breakthrough curves for all sample ports are obtained using both the concentration and ER data (Table 2). The incorporation of both the hydrological and geophysical data into the stochastic inversion procedure therefore results in a valuable improvement in our ability to characterize and predict the hydrological behavior of the system.

Table 2. RMS Difference Between the Mean Predicted Concentration Curves Shown in Figures 6 and 7 and the Corresponding True Curves, Along With the Standard Deviation of All the Predicted Curves, Which Has Been Averaged Over Time[a]

Sample Port Depth (m) and Measure	Prior Distribution	Concentration Data	Resistivity Data	Concentration Plus Resistivity Data
Longer Correlation Length Case (Figure 6)				
1.5: RMS error	13.0	11.3	13.1	**9.0**
1.5: SD	39.6	32.8	28.7	**25.5**
5.5: RMS error	27.7	22.4	22.9	**9.5**
5.5: SD	42.2	34.9	41.1	**33.4**
9.5: RMS error	32.2	**23.8**	36.5	**23.8**
9.5: SD	42.0	29.7	36.6	**30.5**
13.5: RMS error	52.1	16.0	26.0	**10.5**
13.5: SD	45.5	26.5	33.1	**25.1**
Shorter Correlation Length Case (Figure 7)				
1.5: RMS error	10.5	3.7	3.9	**1.5**
1.5: SD	29.6	25.8	21.8	**21.2**
5.5: RMS error	**11.8**	12.9	18.4	14.5
5.5: SD	34.5	27.3	26.4	**25.5**
9.5: RMS error	9.7	6.2	**3.2**	7.9
9.5: SD	35.0	27.1	27.6	**23.0**
13.5: RMS error	**20.9**	23.0	21.7	24.9
13.5: SD	37.0	34.7	33.8	**32.4**

[a]Boldface values represent the smallest values.

[34] For the shorter correlation length example shown in Figure 7, we see results similar to those described above, albeit to a lesser extent than the longer correlation length case. This is despite the fact that the different sets of realizations for this case did not contain many consistent patterns in K connectivity that could be identified through the probability plots in Figure 5. Again, the set of realizations obtained using only the prior information can be seen in Figure 7 to produce predicted concentration curves with a relatively wide spread about the mean. In contrast to the larger correlation length case in Figure 6, however, the spread here is smaller and the true behavior is more accurately matched by the mean prediction. The shorter correlation length K model in Figure 1d contains less significant flow pathways in the subsurface region, and thus the prior realizations tend to provide predictions at the downstream location that are well represented by the average flow and transport behavior of this highly heterogeneous field. Nevertheless, incorporating the concentration and resistivity data independently into the inversion procedure generally results in a reduction of prediction uncertainty, and jointly considering both data sets results in the greatest reduction in this uncertainty when compared to the prior. Thus, even for the shorter correlation length case, the joint inversion of the geophysical and hydrological data allows us to better characterize system behavior, albeit less effectively than in the longer correlation length case.

4. Discussion

[35] Visual inspection of the different sets of realizations obtained with our methodology shows that, by incorporating both the concentration and resistivity data into the stochastic inversion procedure, we can better delineate important subsurface flow pathways in comparison to using either data type alone. This is especially the case for the longer correlation length model considered. More importantly, predictions of a notably different tracer injection/extraction experiment through the simulation region showed a reduction in variance and an excellent mean prediction when both data types were used together. Again, this was especially true for the longer correlation length case, as in the shorter correlation length case with smaller-scale heterogeneity, flow and transport are not as controlled by preferential pathways.

[36] The examples we have presented, which we feel provide an important proof of concept for the identification of K heterogeneity using fully stochastic methods with simplified parameterizations, were run in 2-D and are small in scale because of the computational expense of the Bayesian MCMC approach. As mentioned, running each of our inversions to generate 150,000 accepted realizations took ~1 week of CPU time. The computational expense increases greatly when the 3-D nature of flow and transport in the field is considered, and thus application to field data has not yet been attempted. One potential solution to this dimensionality problem is to make use of parallel computation. For the MCMC approach utilized here, where the accepting or rejecting of proposed configurations depends on the previously accepted configuration, parallelization is not as straightforward as with other stochastic inversion approaches like the generalized likelihood uncertainty estimation (GLUE) technique, where random models are generated and accepted/rejected independently of one another [e.g., *Beven and Binley*, 1992; *Binley and Beven*, 2003; *Cassiani et al.*, 2004; *Cassiani and Binley*, 2005; *Looms et al.*, 2008]. Nevertheless, individual forward models could be parallelized with the MCMC approach to significantly reduce the computation time [*Aines et al.*, 2002]. In addition, multiple MCMC chains can be run simultaneously on different processors, which can then be used to efficiently determine the burn-in period, and after burn-in to rapidly generate feasible posterior configurations. Finally, much promise lies in the idea of letting the results of parallel MCMC chains adaptively refine the prior distribution as the algorithm runs for greatly increased speed. This is the idea behind the Differential Evolution Adaptive Metropolis (DREAM) approach of *Vrugt et al.* [2009], which might be adapted for use in a problem similar to that shown here. One issue with the DREAM approach that will need to be

addressed, however, is ensuring that hybrid proposal configurations, which are derived from the results of multiple parallel chains, still agree with the prior information in terms of the specified correlation structure between model cells.

[37] Another potential strategy to improve the speed of the Bayesian MCMC methodology would be to develop more clever parameterizations or incorporate greater amounts of prior information, such that we limit even further the number of possible subsurface configurations. To this end, one possibility would be to include more information regarding the spatial configuration of facies, which might be obtained from cluster analysis of multiple inverted geophysical images [*Moysey et al.*, 2003; *Tronicke et al.*, 2004; *Paasche et al.*, 2006]. Other hard data such as facies information at the borehole locations could also be integrated into the prior distribution if available. Using approximate forward models is yet another means of increasing the speed of the MCMC procedure. For example, we could consider particle tracking rather than solving the advective-dispersive equation with a finite difference method as was done here to simulate transport, or perhaps use a polynomial chaos expansion to greatly reduce the time required for forward model computations [e.g., *Balakrishnan et al.*, 2003]. We could also reduce the number of resistivity current pairs, thereby reducing the number of electrical forward runs required.

[38] One final important issue that requires discussion is the validity of the uncertainty estimates obtained using the Bayesian MCMC methodology. Until now, we have made no attempt to address the difficult issue of data and model errors with such methods, which control the prediction uncertainty estimates obtained from the generated sets of realizations. In theory, if the geophysical and hydrological models used in the inversion procedure were perfect, then the data uncertainties input into the algorithm through the likelihood equations could be simply prescribed, at least in this synthetic case, to the 5% uncorrelated Gaussian errors that were added to both the concentration and apparent resistivity data. However, in any realistic situation, and especially because of the simplifying assumptions we use to make the spatially distributed inverse problem computationally feasible, model structural errors are present. These errors effectively act together with the data errors to produce substantial, correlated differences between the true, error-free data sets and those produced by the best (but approximate) model. Practically, what this means is that data uncertainties will need to have significantly higher variances than the data measurement errors for the MCMC algorithm to properly function. In addition, because of the computational expense of the MCMC procedure, it may be desirable to prescribe larger data error variances such that the algorithm is able to generate posterior realizations in a reasonable time frame. All of this leaves practitioners of MCMC methods in a difficult position in terms of properly assessing posterior uncertainty because, in a sense, the prescribed data errors can seem somewhat subjective [e.g., *Vrugt and Bouten*, 2002]. A possible partial solution might be to run the procedure considering multiple error models and examine the resulting realizations. Another possibility would be to attempt to estimate error model parameters, including correlation, in the procedure itself. Despite these limitations, our work demonstrates that the incorporation of time-lapse geophysical data into the subsurface characterization problem allows for the identification of fast flowpaths and reduced uncertainty in future hydrological predictions, even when the effective data errors are largely unknown. Further information about the data and model error structure can only improve the results that have been presented here.

5. Conclusions

[39] The results presented in this paper demonstrate that MCMC methods provide a potentially powerful framework within which to integrate, in a fully stochastic manner, dynamic ER data for the estimation of hydrological properties. Whereas previous research involving stochastic inversion methods in hydrogeophysics has primarily involved the estimation of a small number of average subsurface parameters using fast 1-D models, here we estimate spatially distributed properties to capture connected heterogeneity in hydraulic conductivity. This comes at the cost of being computationally expensive, which means that novel simplifying prior assumptions are necessary to make the problem computationally tractable. Key considerations made in our work with ER and solute concentration data were that (1) we are dealing with a binary K system where the mean K and porosity values are known, when in fact the true K distribution varies continuously; (2) we have limited information regarding the correlation structure of the two facies; and (3) an Archie-type relation with unknown m exponent links solute concentration to resistivity. The primary advantage of a fully stochastic approach to inversion is that it allows us to explore the nonlinearity and nonuniqueness of the coupled problem and the associated model parameter and prediction uncertainties.

[40] **Acknowledgments.** We sincerely thank Klaus Holliger and the Faculty of Earth and Environmental Sciences at the University of Lausanne for the financial support of K.S. during her visits to Switzerland in 2008 and 2009. This work was funded in part by NSF grant EAR-0747629.

References

Adams, E., and L. Gelhar (1992), Field study of dispersion in a heterogeneous aquifer: 2. Spatial moments analysis, *Water Resour. Res.*, *28*, 3293–3307, doi:10.1029/92WR01757.

Aines, R., et al. (2002), The stochastic engine initiative: Improving prediction of behavior in geologic environments we cannot directly observe, *Rep. UCRL-ID-148221*, 58 pp., Lawrence Livermore Natl. Lab., Livermore, Calif.

Archie, G. E. (1942), The electrical resistivity log as an aid in determining some reservoir characteristics, *Trans. Am. Inst. Min. Metall. Pet. Eng.*, *146*, 54–62.

Balakrishnan, S., A. Roy, M. G. Ierapetritou, G. P. Flach, and P. G. Georgopoulos (2003), Uncertainty reduction and characterization for complex environmental fate and transport models: An empirical Bayesian framework incorporating the stochastic response surface method, *Water Resour. Res.*, *39*(12), 1350, doi:10.1029/2002WR001810.

Beckie, R. (1996), Measurement scale, network sampling scale, and groundwater model parameters, *Water Resour. Res.*, *32*, 65–76, doi:10.1029/95WR02921.

Beres, M., and F. P. Haeni (1991), Application of ground-penetrating-radar methods in hydrogeologic studies, *Ground Water*, *29*, 375–386, doi:10.1111/j.1745-6584.1991.tb00528.x.

Beven, K., and A. Binley (1992), Future of distributed models: Model calibration and uncertainty prediction, *Hydrol. Process.*, *6*, 279–298, doi:10.1002/hyp.3360060305.

Binley, A., and K. Beven (2003), Vadose zone flow model uncertainty as conditioned on geophysical data, *Ground Water*, *41*, 119–127, doi:10.1111/j.1745-6584.2003.tb02576.x.

Binley, A., G. Cassiani, R. Middleton, and P. Winship (2002), Vadose zone flow model parameterisation using cross-borehole radar and resistivity

imaging, *J. Hydrol. Amsterdam*, *267*, 147–159, doi:10.1016/S0022-1694(02)00146-4.

Bosch, M. (1999), Lithologic tomography: From plural geophysical data to lithology estimation, *J. Geophys. Res.*, *104*, 749–766, doi:10.1029/1998JB900014.

Cassiani, G., and A. Binley (2005), Modeling unsaturated flow in a layered formation under quasi-steady state conditions using geophysical data constraints, *Adv. Water Resour.*, *28*, 467–477, doi:10.1016/j.advwatres.2004.12.007.

Cassiani, G., G. Böhm, A. Vesnaver, and R. Nicolich (1998), A geostatistical framework for incorporating seismic tomography auxiliary data into hydraulic conductivity estimation, *J. Hydrol. Amsterdam*, *206*, 58–74, doi:10.1016/S0022-1694(98)00084-5.

Cassiani, G., C. Strobbia, and L. Galloti (2004), Vertical radar profiles for the characterization of deep vadose zones, *Vadose Zone J.*, *3*, 1093–1105, doi:10.2113/3.4.1093.

Chen, J., S. Hubbard, and Y. Rubin (2001), Estimating the hydraulic conductivity at the South Oyster Site from geophysical tomographic data using Bayesian techniques based on the normal linear regression model, *Water Resour. Res.*, *37*, 1603–1613, doi:10.1029/2000WR900392.

Chen, J., S. S. Hubbard, K. H. Williams, S. Pride, L. Li, C. Steefel, and L. Slater (2009), A state-space Bayesian framework for estimating biogeochemical transformations using time-lapse geophysical data, *Water Resour. Res.*, *45*, W08420, doi:10.1029/2008WR007698.

Day-Lewis, F. D., J. W. Lane Jr., J. M. Harris, and S. M. Gorelick (2003), Time-lapse imaging of saline-tracer transport in fractured rock using difference-attenuation radar tomography, *Water Resour. Res.*, *39*(10), 1290, doi:10.1029/2002WR001722.

Day-Lewis, F. D., K. Singha, and A. M. Binley (2005), Applying petrophysical models to radar travel time and electrical-resistivity tomograms: Resolution-dependent limitations, *J. Geophys. Res.*, *110*, B08206, doi:10.1029/2004JB003569.

Deutsch, C. V., and A. G. Journel (1992), *GSLIB: Geostatistical Software Library and User's Guide*, Oxford Univ. Press, New York.

Doyen, P. M. (1988), Porosity from seismic data: A geostatistical approach, *Geophysics*, *53*, 1263–1276, doi:10.1190/1.1442404.

Eidsvik, J., H. Omre, T. Mukerji, G. Mavko, P. Avseth, and N. Hydro (2002), Seismic reservoir prediction using Bayesian integration of rock physics and Markov random fields: A North Sea example, *Leading Edge*, *21*, 290–294, doi:10.1190/1.1463780.

Ezzedine, S., Y. Rubin, and J. S. Chen (1999), Bayesian method for hydrogeological site characterization using borehole and geophysical survey data: Theory and application to the Lawrence Livermore National Laboratory Superfund site, *Water Resour. Res.*, *35*, 2671–2683, doi:10.1029/1999WR900131.

Ferré, T., L. Bentley, A. Binley, N. Linde, A. Kemna, K. Singha, K. Holliger, J. A. Huisman, and B. Minsley (2009), Critical steps for the continuing advancement of hydrogeophysics, *Eos Trans. AGU*, *90*(23), doi:10.1029/2009EO230004.

Finsterle, S., and M. Kowalsky (2008), Joint hydrological-geophysical inversion for soil structure identification, *Vadose Zone J.*, *7*, 287–293, doi:10.2136/vzj2006.0078.

Garambois, S., P. Sénéchal, and H. Perroud (2002), On the use of combined geophysical methods to assess water content and water conductivity of near-surface formations, *J. Hydrol. Amsterdam*, *259*, 32–48, doi:10.1016/S0022-1694(01)00588-1.

Gelman, A., and D. Rubin (1992), Inference from iterative simulation using multiple sequences, *Stat. Sci.*, *7*, 457–472, doi:10.1214/ss/1177011136.

Goovaerts, P. (1997), *Geostatistics for Natural Resources Evaluation*, Oxford Univ. Press, New York.

Harbaugh, A. W., E. R. Banta, M. C. Hill, and M. G. McDonald (2000), MODFLOW-2000, the U.S. Geological Survey modular ground-water model: User guide to modularization concepts and the ground-water flow process, *U.S. Geol. Surv. Open File Rep., 00-92*, 1–121.

Hess, K. M., S. H. Wolf, and M. A. Celia (1992), Large-scale natural gradient tracer test in sand and gravel, Cape Cod, Massachusetts: 3. Hydraulic conductivity variability and calculated macrodispersivities, *Water Resour. Res.*, *28*, 2011–2027, doi:10.1029/92WR00668.

Hinnell, A. C., T. P. A. Ferré, J. A. Vrugt, J. A. Huisman, S. Moysey, J. Rings, and M. B. Kowalsky (2010), Improved extraction of hydrologic information from geophysical data through coupled hydrogeophysical inversion, *Water Resour. Res.*, *46*, W00D40, doi:10.1029/2008WR007060.

Huang, X., L. Meister, and R. Workman (1997), Reservoir characterization by integration of time-lapse seismic and production data, paper presented at Annu. Tech. Conf. and Exhib., Soc. Petrol. Eng., San Antonio, Tex., 5–8 Oct.

Hubbard, S. S., and Y. Rubin (2005), *Hydrogeophysics*, Springer, New York.

Hubbard, S. S., J. Chen, J. Peterson, E. L. Majer, K. H. Williams, D. J. Swift, B. Mailloux, and Y. Rubin (2001), Hydrogeological characterization of the South Oyster bacterial transport site using geophysical data, *Water Resour. Res.*, *37*, 2431–2456, doi:10.1029/2001WR000279.

Hyndman, D. W., and S. M. Gorelick (1996), Estimating lithologic and transport properties in three dimensions using seismic and tracer data: The Kesterson Aquifer, *Water Resour. Res.*, *32*, 2659–2670, doi:10.1029/96WR01269.

Hyndman, D. W., and J. M. Harris (1996), Traveltime inversion for the geometry of aquifer lithologies, *Geophysics*, *61*, 1728–1737, doi:10.1190/1.1444090.

Hyndman, D. W., J. M. Harris, and S. M. Gorelick (1994), Coupled seismic and tracer test inversion for aquifer property characterization, *Water Resour. Res.*, *30*, 1965–1977, doi:10.1029/94WR00950.

Hyndman, D. W., J. M. Harris, and S. M. Gorelick (2000), Inferring the relation between seismic slowness and hydraulic conductivity in heterogeneous aquifers, *Water Resour. Res.*, *36*, 2121–2132, doi:10.1029/2000WR900112.

Jadoon, K., E. Slob, M. Vanclooster, H. Vereecken, and S. Lambot (2008), Uniqueness and stability analysis of hydrogeophysical inversion for time-lapse ground penetrating radar estimates of shallow soil hydraulic properties, *Water Resour. Res.*, *44*, W09421, doi:10.1029/2007WR006639.

Keller, G. V., and F. C. Frischknecht (1966), *Electrical Methods in Geophysical Prospecting*, Pergamon, Oxford, U. K.

Kemna, A., J. Vanderborght, B. Kulessa, and H. Vereecken (2002), Imaging and characterisation of subsurface solute transport using electrical resistivity tomography (ERT) and equivalent transport models, *J. Hydrol. Amsterdam*, *267*, 125–146, doi:10.1016/S0022-1694(02)00145-2.

Knight, R. J., and A. L. Endres (2005), An introduction to rock physics for near-surface applications, in *Near-Surface Geophysics*, vol. 1, *Concepts and Fundamentals*, pp. 31–70, Soc. of Explor. Geophys., Tulsa, Okla.

Knudby, C., and J. Carrera (2005), On the relationship between indicators of geostatistical flow and transport connectivity, *Adv. Water Resour.*, *28*, 405–421.

Koestel, J., A. Kemna, M. Javaux, A. Binley, and H. Vereecken (2008), Quantitative imaging of solute transport in an unsaturated and undisturbed soil monolith with 3-D ERT and TDR, *Water Resour. Res.*, *44*, W12411, doi:10.1029/2007WR006755.

Kowalsky, M. B., S. Finsterle, and Y. Rubin (2004), Estimating flow parameter distributions using ground-penetrating radar and hydrological measurements during transient flow in the vadose zone, *Adv. Water Resour.*, *27*, 583–599, doi:10.1016/j.advwatres.2004.03.003.

Kowalsky, M., S. Finsterle, J. Peterson, S. Hubbard, Y. Rubin, E. Majer, A. Ward, and G. Gee (2005), Estimation of field-scale soil hydraulic and dielectric parameters through joint inversion of GPR and hydrological data, *Water Resour. Res.*, *41*, W11425, doi:10.1029/2005WR004237.

Kretz, V., M. Le Ravalec-Dupin, and F. Roggero (2004), An integrated reservoir characterization study matching production data and 4D seismic, *SPE Reservoir Eval. Eng.*, *7*, 116–122, doi:10.2118/88033-PA.

Lambot, S., M. Antoine, I. Van den Bosch, E. Slob, and M. Vanclooster (2004), Electromagnetic inversion of GPR signals and subsequent hydrodynamic inversion to estimate effective vadose zone hydraulic properties, *Vadose Zone J.*, *3*, 1072–1081, doi:10.2113/3.4.1072.

Lambot, S., E. Slob, M. Vanclooster, and H. Vereecken (2006), Closed loop GPR data inversion for soil hydraulic and electric property determination, *Geophys. Res. Lett.*, *33*, L21405, doi:10.1029/2006GL027906.

Lehikoinen, A., S. Finsterle, A. Voutilainen, M. Kowalsky, and J. Kaipio (2009), Dynamical inversion of geophysical ERT data: State estimation in the vadose zone, *Inverse Probl. Sci. Eng.*, *17*, 715–736, doi:10.1080/17415970802475951.

Linde, N., A. Binley, A. Tryggvason, L. Pedersen, and A. Revil (2006a), Improved hydrogeophysical characterization using joint inversion of cross-hole electrical resistance and ground-penetrating radar travel time data, *Water Resour. Res.*, *42*, W12404, doi:10.1029/2006WR005131.

Linde, N., S. Finsterle, and S. Hubbard (2006b), Inversion of tracer test data using tomographic constraints, *Water Resour. Res.*, *42*, W04410, doi:10.1029/2004WR003806.

Linde, N., A. Revil, A. Boleve, C. Dages, J. Castermant, B. Suski, and M. Voltz (2007), Estimation of the water table throughout a catchment using self-potential and piezometric data in a Bayesian framework, *J. Hydrol. Amsterdam*, *334*, 88–98, doi:10.1016/j.jhydrol.2006.09.027.

Looms, M. C., A. Binley, K. H. Jensen, L. Nielsen, and T. M. Hansen (2008), Identifying unsaturated hydraulic parameters using an integrated data fusion approach on cross-borehole geophysical data, *Vadose Zone J.*, *7*, 238–248, doi:10.2136/vzj2007.0087.

Mavko, G., T. Mukerji, and J. Dvorkin (1998), *The Rock Physics Handbook*, Cambridge Univ. Press, Cambridge, U. K.

McKenna, S. A., and E. P. Poeter (1995), Field example of data fusion in site characterization, *Water Resour. Res.*, *31*, 3229–3240, doi:10.1029/95WR02573.

Metropolis, N., A. Rosenbluth, M. Rosenbluth, A. Teller, and E. Teller (1953), Equation of state calculations by fast computing machines, *J. Chem. Phys.*, *21*, 1087–1092, doi:10.1063/1.1699114.

Mosegaard, K., and A. Tarantola (1995), Monte Carlo sampling of solutions to inverse problems, *J. Geophys. Res.*, *100*, 12,431–12,448, doi:10.1029/94JB03097.

Moysey, S., and R. J. Knight (2004), Modeling the field-scale relationship between dielectric constant and water content in heterogeneous systems, *Water Resour. Res.*, *40*, W03510, doi:10.1029/2003WR002589.

Moysey, S., J. Caers, R. Knight, and R. Allen-King (2003), Stochastic estimation of facies using ground penetrating radar data, *Stochastic Environ. Res. Risk Assess.*, *17*, 306–318, doi:10.1007/s00477-003-0152-6.

Moysey, S., K. Singha, and R. Knight (2005), A framework for inferring field-scale rock physics relationships through numerical simulation, *Geophys. Res. Lett.*, *32*, L08304, doi:10.1029/2004GL022152.

Mukerji, T., A. Jorstad, P. Avseth, G. Mavko, and J. R. Granli (2001), Mapping lithofacies and pore-fluid probabilities in a North Sea reservoir: Seismic inversions and statistical rock physics, *Geophysics*, *66*, 988–1001, doi:10.1190/1.1487078.

Paasche, H., J. Tronicke, K. Holliger, A. Green, and H. Maurer (2006), Integration of diverse physical-property models: Subsurface zonation and petrophysical parameter estimation based on fuzzy c-means cluster analyses, *Geophysics*, *71*, H33–H44, doi:10.1190/1.2192927.

Pidlisecky, A., and R. Knight (2008), FW2_5D: A MATLAB 2.5-D electrical resistivity modeling code, *Comput. Geosci.*, *34*, 1645–1654, doi:10.1016/j.cageo.2008.04.001.

Poeter, E., and D. Gaylord (1990), Influence of aquifer heterogeneity on contaminant transport at the Hanford Site, *Ground Water*, *28*, 900–909, doi:10.1111/j.1745-6584.1990.tb01726.x.

Prasad, M. (2003), Velocity-permeability relations within hydraulic units, *Geophysics*, *68*, 108–117, doi:10.1190/1.1543198.

Ramirez, A. L., J. J. Nitao, W. G. Hanley, R. Aines, R. E. Glaser, S. K. Sengupta, K. M. Dyer, T. L. Hickling, and W. D. Daily (2005), Stochastic inversion of electrical resistivity changes using a Markov Chain Monte Carlo approach, *J. Geophys. Res.*, *110*, B02101, doi:10.1029/2004JB003449.

Scheibe, T., and S. Yabusaki (1998), Scaling of flow and transport behavior in heterogeneous groundwater systems, *Adv. Water Resour.*, *22*, 223–238, doi:10.1016/S0309-1708(98)00014-1.

Schön, J. H. (1998), *Physical Properties of Rocks: Fundamentals and Principles of Petrophysics*, Pergamon, New York.

Singha, K., and S. M. Gorelick (2005), Saline tracer visualized with electrical resistivity tomography: Field scale moment analysis, *Water Resour. Res.*, *41*, W05023, doi:10.1029/2004WR003460.

Singha, K., and S. M. Gorelick (2006), Hydrogeophysical tracking of 3D tracer migration: The concept and application of apparent petrophysical relations, *Water Resour. Res.*, *42*, W06422, doi:10.1029/2005WR004568.

Singha, K., F. Day-Lewis, and S. Moysey (2007), Accounting for tomographic resolution in estimating hydrologic properties from geophysical data, in *Subsurface Hydrology: Data Integration for Properties and Processes*, *Geophys. Monogr. Ser.*, vol. 171, edited by D. W. Hyndman, F. D. Day-Lewis, and K. Singha, pp. 227–242, AGU, Washington, D. C.

Topp, G., J. Davis, and A. Annan (1980), Electromagnetic determination of soil water content: Measurements in coaxial transmission lines, *Water Resour. Res.*, *16*, 574–582, doi:10.1029/WR016i003p00574.

Tronicke, J., K. Holliger, W. Barrash, and M. Knoll (2004), Multivariate analysis of cross-hole georadar velocity and attenuation tomograms for aquifer zonation, *Water Resour. Res.*, *40*, W01519, doi:10.1029/2003WR002031.

Vrugt, J., and W. Bouten (2002), Validity of first-order approximations to describe parameter uncertainty in soil hydrologic models, *Soil Sci. Soc. Am. J.*, *66*, 1740–1751.

Vrugt, J., C. ter Braak, C. Diks, B. Robinson, J. Hyman, and D. Higdon (2009), Accelerating Markov Chain Monte Carlo simulation by differential evolution with self-adaptive randomized subspace sampling, *Int. J. Nonlinear Sci. Numer. Simul.*, *10*, 1–12.

Wen, X., and J. Gómez-Hernández (1998), Numerical modeling of macrodispersion in heterogeneous media: A comparison of multi-Gaussian and non-multi-Gaussian models, *J. Contam. Hydrol.*, *30*, 129–156, doi:10.1016/S0169-7722(97)00035-1.

Wen, X., S. Lee, and T. Yu (2006), Simultaneous integration of pressure, water cut, 1- and 4-D seismic data in geostatistical reservoir modeling, *Math. Geol.*, *38*, 301–325, doi:10.1007/s11004-005-9016-6.

Zheng, C., and S. Gorelick (2003), Analysis of solute transport in flow fields influenced by preferential flowpaths at the decimeter scale, *Ground Water*, *41*, 142–155, doi:10.1111/j.1745-6584.2003.tb02578.x.

Zheng, C., and P. P. Wang (1999), MT3DMS: A modular three-dimensional multispecies model for simulation of advection, dispersion and chemical reactions of contaminants in groundwater systems: Documentation and user's guide, *Contract Rep. SERDP-99-1*, 202 pp., U.S. Army Eng. Res. and Dev. Cent., Vicksbug, Miss.

J. Irving, School of Engineering, University of Guelph, Guelph, Ontario N1G 2W1, Canada. (irvingj@uoguelph.ca)

K. Singha, Department of Geosciences, Pennsylvania State University, 311 Deike Building, University Park, PA 16802, USA.